Journal of Engineering Science and Technology
23rd EURECA 2025 Special Issue February (2026) 63 - 80


# DESIGN AND ANALYSIS OF A CONTACTLESS AIR CONVEYOR

YONG CHUN SIAH, DOUGLAS TONG KUM TIEN*

School of Engineering, Faculty of Innovation and Technology,
Taylor's University, Subang Jaya, Selangor, Malaysia
*Corresponding Author: DouglasKumTien.Tong@taylors.edu.my

## Abstract

Contactless air conveyors are increasingly utilized in modern industries to handle fragile and contamination-sensitive products, enabling precise, high-speed transportation without physical contact. Existing systems such as air-cushion conveyors based on pneumatic levitation or aerodynamic traction, offer viable solutions; however, they often face limitations in stability, energy efficiency, and scalability. This study aims to develop a novel contactless air conveyor system utilizing a modular array of hexagonal actuators to enable multidirectional movement and uniform pressure distribution. Key parameters including airflow rate, pressure differential, and geometry were evaluated to enhance performance and energy efficiency. To achieve this, the study combined Computational Fluid Dynamics (CFD) simulations in ANSYS Fluent with analytical modelling in MATLAB to optimize geometric parameters. Validation was performed through comparison with literature benchmarks and analytical modelling to verify the accuracy of CFD simulations. Key findings indicated that the hexagonal actuator has improved traction force and enables enhanced acceleration and multidirectional movement. However, this improvement was accompanied by higher airflow demands, indicating increased power consumption. Parametric studies demonstrated that the pressure difference has the most significant impact on performance, while actuator geometry configuration offered additional tuning capabilities for balancing force generation and energy efficiency. Moreover, balanced port configurations and moderate pocket depths improved traction and vertical lifting force, supporting the feasibility of the design. Future work will focus on prototype development, experimental validation, and the development of control strategies for 6-DOF manipulation and energy-efficient operation.

Keywords: Aerodynamic-traction, Contactless conveyor, Energy efficiency, Multidirectional object movement, Pneumatic levitation.

# 1. Introduction

Product handling and positioning are critical processes in the industry to transport and manipulate parts and products between multiple stages and locations. A conveyor system is an effective approach that is utilized for production transferring or positioning, enabling continuous product movement, and eliminating downtime. Contactless transport approaches were introduced and proven to be effective in eliminating physical contact and reducing the risk throughout the conveying process for fragile and clean products. This includes glass sheets, silicon wafers, etc, which necessitate careful handling and precise positioning. Chanduet et al. [1] highlighted that contactless conveyors play a critical role in semiconductor manufacturing and food handling processes due to its ability to prevent contamination and product damage.

To achieve zero physical contact between products and the conveyor, various contactless approaches have been introduced and can be categorized into magnetic, electrostatic, near field, and pneumatic levitation [2]. The pneumatic levitation method emerged as particularly noteworthy, offering a wide range of applications due to being clean, magnetic-free free and causing minimal heat generation [3]. In theory, a contactless conveyor system typically requires two key forces, which are levitation (bearing) to lift and support the object, and propulsion (motor) to control movement while suspended [4]. The primary difference between contactless conveyor approaches depends on how these forces are generated and the specific roles they fulfil within the system.

For instance, the electromagnetic levitation method implements contactless actuation by producing lift and propulsion through the interaction of magnetic and electric fields, thus it is limited only to ferromagnetic or electrically conductive items [5]. Conversely, pneumatic levitation has been proposed as an alternative technology to address the limitations of the previous method. It offers cleanliness, a non-magnetic nature, and minimal heat generation. The system works by creating a pressure difference between the object's top and bottom surfaces to counteract gravity [6]. Pneumatic levitation is primarily divided into two approaches, which are the Bernoulli vacuum and air-cushion methods. The Bernoulli vacuum method lifts flat objects by applying suction force to the objects. However, it is less suitable for handling fragile items due to the potential safety risk, such as grip loss from gaps and frequent wear of the rubber ring that might cause breakage [7, 8]. The air-cushion method levitates objects by employing pressurized air through designed nozzles or chambers, thus forming a stable cushion beneath the object. Although it is effective for vertical levitation, it lacked horizontal transport capability since the airflow was directed perpendicularly. Subsequently, the inclined air jets and the aerodynamic-traction principle were introduced.

## Principles of contactless air conveyors

Inclined air nozzle and aerodynamics-traction approaches enable both levitation and actuation functions without contact between the object and the conveyor. The inclined air jets method involves directing a pressurized airflow through an array of tilted nozzles to create shear that levitates and propels the objects, as shown in Fig. 1. It was first implemented in the 1970s by Paivanas and Hassan [9] for handling fragile semiconductor wafers. Although it reduced contact, external support was still required for stability and control. To improve control, Konishi and

Fujita [10] developed a system using fluidic micro-actuators regulated by electrostatic forces, enabling dynamic airflow direction control. Subsequently, a Microelectromechanical System (MEMS)-based actuator system for micro-product manipulation was proposed by Fukuta et al. [11]. It used adjustable control valves to manipulate airflow orientation depending on the applied voltage and was successfully proven with a transport speed of 4.5 mm/s. More recently, Zeggari et al. [12] developed a MEMS-based two-dimensional micro-conveyor capable of multidirectional movement using tilted air jets. Although the system was effective for flat substrates, its scalability and precise positioning were limited.

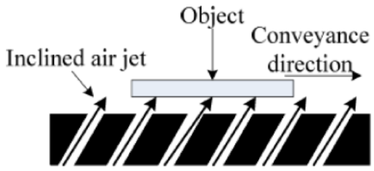


**Fig. 1. Titled air-jet method [5].**

To meet the increasing complexity of transporting fragile and lightweight components, pressure field manipulation for contactless conveyance were explored. Chen and DeBra [8] and Delhaes et al. [13] employed viscous forces to produce linear motion. Delettre et al. [14] developed a conveyor system armed with individually controlled vertical air jets to levitate and drive items through surrounding airflow, thereby driving and manipulating the movement of the object without touching. A major advancement was introduced by van Rij et al. [15], which a novel actuator cell array system that leveraged on the aerodynamic-traction concept. This system generated shear forces for object movement by applying differential pressure between positive and negative ports, as illustrated in Fig. 2. A modified version based on the early design introduced by van Rij et al. [16] was subsequently proposed and was proven to improve traction forces through more uniform pressure distribution due to the addition of grooves that connected adjacent ports.

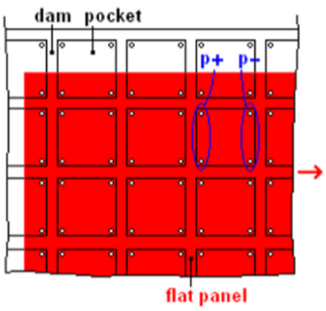


**Fig. 2. Actuator cell positioned in the conveyor surface [15].**

Based on these advancements, van Ostayen et al. [17] and Wesselingh [18] introduced a 6-DOF contactless transport system using two opposing actuator arrays. By precisely controlling supply pressures in actuator pairs, multi-axis motion and stable levitation were achieved. Further innovation in design came from Vuong [4], who developed the flowerbed actuator system by using tiltable hexagonal cells with a flexible intermediate plate to dynamically adjust pressure distribution. The system offered stable, multi-degree-of-freedom control. Building upon this research, Krijnen et al. [19] implemented fractional-order PID control to achieve precise, contactless positioning of fragile substrates like silicon wafers, with efforts to enhance industrial applicability.

However, these current approaches still face specific limitations that restrict their application across diverse industrial settings. These constraints consist of material specificity, scalability, energy efficiency, handling capability, and building costs. For example, Delettre et al. [14] demonstrated vertical air-jet based contactless transport, but the system offered only one-dimensional control and required complex valve regulation, limiting dynamic applications. Similarly, Vuong [4] developed a "Flowerbed" actuator system that enabled precise 3-DOF movement, but its complex manifold structure reduced scalability and responsiveness, and the overall system remained costly. Hence, the objectives of this study are as follows.

- To design a contactless air conveyor that is suitable for a diverse range of industrial practices to overcome the present limitations.
- To analyse the effects of key design parameters—such as actuator geometry, pressure differential, and airflow configuration—on system performance through simulation.

This study aims to contribute to the development of a reliable, scalable, and cost-effective contactless transport solution suitable for modern industrial applications.

## 2. Research Methodology

A structured methodology consisting of four different stages, including model validation, design ideation, design modelling, and computational simulation was undertaken. The goal was to develop and optimize a novel contactless air conveyor system, called the HexaFloat system, by utilizing the aerodynamic-traction principles to achieve precise contactless transportation for delicate objects. Each of these stages focused on validating the effectiveness of this novel HexaFloat system in terms of its stability, levitation, and directional control.

### 2.1. Model validation

The model validation was conducted by replicating and analysing a previously published actuator model using ANSYS Fluent and MATLAB analytical modelling. The actuator design and governing equations proposed by van Rij et al. [16] which leveraged aerodynamic-traction principles for contactless wafer transport were chosen for model validation as shown in Fig. 3. The purpose of validation was to verify that the simulation and analytical methods used were consistent with established literature standards before applying them to the novel design. It also helped identify any modelling or simulation setup errors, thus ensuring the accuracy and reliability of the model. Parameters such as pressure distribution, velocity, volume flow rate, and traction force were evaluated and compared against the simulation and analytical predictions using the simplified Navier–Stokes and Reynolds equations mentioned in the literature.

To ensure the accuracy and reliability of the CFD simulation in ANSYS Fluent, the Tetrahedral mesh type was employed due to the complex geometry of the actuator pocket. The mesh quality was controlled carefully with a maximum skewness kept below 0.95, based on the best practices for numerical stability. An inflation layer was applied to the thin air film region between the actuator surface and the levitated object to accurately capture near-wall flow characteristics and shear forces. This was essential for resolving the pressure and velocity gradients critical to the aerodynamic-traction mechanism. A hybrid initialization method was used to accelerate convergence, and the residual criteria for all governing equations were set to $1\times10^{-5}$ to ensure numerical accuracy. The simulation utilized the SIMPLE algorithm solver for pressure–velocity coupling as it provided a stable and efficient method for steady-state, incompressible flows commonly encountered in low-speed aerodynamic applications such as contactless air conveyors.

The reference actuator array used for validation consisted of 30 square cells with a side length L=12.5 mm, characterized by non-dimensional parameters α (pocket length) and β (pocket depth). α represents the proportion of the actuator cell length occupied by the central pocket region, influencing the pressure distribution and flow profile across the actuator. β defines the ratio between the film height over the dam and the film height in the pocket, affecting the shear generation and traction force on the levitated object. The air film height (h) was fixed at 35 µm. Geometric details are provided in Table 1. The flow was modelled as incompressible, isothermal, and laminar (Re < 10), with the analytical model using thin-film approximations of the incompressible Navier–Stokes equations under the assumption of uniform pressure distribution. For CFD validation, a 3×3 array (9 cells) was simulated in ANSYS Fluent using the same geometry and pressure differences of 0.25 kPa, 0.5 kPa, and 1 kPa. Boundary conditions included pressure inlets and outlets at ports, symmetry on lateral faces to mimic array repetition, and no-slip conditions on the top (wafer) and actuator surfaces.

**Table 1. Dimension for validation model [16].**

| Parameters | Explanation | Unit | Value |
|---|---|---|---|
| $\beta$ | Pocket Depth Ratio | - | 0.46 |
| $\alpha$ | Actuator Pocket Length Ratio | - | 0.8 |
| $d_{in}$ | Input port diameter | mm | 0.4 |
| $d_{out}$ | Output port diameter | mm | 1 |

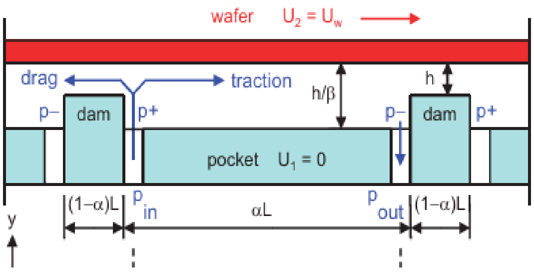


**Fig. 3. Schematic geometry of validation model [16].**

The traction forces $(F_x)$ and volume flow rate $(Q)$ for each design parameter was determined by using the theoretical equation proposed by van Rij et al. [16], as described below:

$$Q = \left(\frac{1}{\beta^3\alpha} + \frac{1}{(1-\alpha)}\right)\frac{h^3}{12\mu}\cdot\frac{\Delta pB}{L} + \left(\frac{1}{\beta} - 1\right)\frac{U_w hB}{2}\#(1) \quad (1)$$

$$F_x = \left(\frac{h}{2\beta}\frac{\Delta p}{\alpha L} - \frac{\mu U_w \beta}{h}\right)(\alpha LB) + \left(-\frac{h}{2}\frac{\Delta p}{(1-\alpha)L} - \frac{\mu U_w}{h}\right)\big((1-\alpha)LB\big)\#(2) \quad (2)$$

where, $\mu$ is the air viscosity, $U_w$ is the wafer velocity, and B is the pocket width.

## 2.2. Design ideation

Innovative actuator geometries were conceptualized to improve pressure uniformity and enable multidirectional control by transforming square actuator cells to hexagonal shape. This change reduced dead zones and able to support six-DOF (Degree of freedom) movement. Drawing insight from the model introduced by van Rij et al. [16], this design focused on enhancing system performance through geometric modification.

Previous works, such as van Rij et al. [16], demonstrated the feasibility of square actuator arrays but were limited by uneven pressure distribution and restricted multidirectional control. van Ostayen et al. [17] advanced the concept with improved six-DOF manipulation however the design still suffered from geometric asymmetry and gaps between actuators, leading to inefficiencies in continuous transport.

Building upon these insights, a novel system named HexaFloat was designed based on the aerodynamic traction principle. The key innovation lies in adopting a modular hexagonal actuator cell array, which provides superior geometric symmetry, reduces inter-actuator gaps, and enables smoother multidirectional transitions. It is anticipated that the integration of a valve-based control algorithm into this modular design can offer precise directional airflow control and improve responsiveness compared to earlier systems. The finalized geometry of the HexaFloat is shown in Section 2.3

## 2.3. Design modelling

Upon the model being validated against literature, design parameters for model simulation were to be determined. The initial step involved identifying system requirements for transporting and precise positioning flat and delicate products such as silicon wafers and glass substrates. According to van Rij et al. [16], the typical wafer diameters ranged from 100 mm to 450 mm, while glass substrates may exceed 2 m² in area, with both having thicknesses of around 0.7 mm. Key system-level performance targets were identified to guide the design process, summarized in Table 2.

These targets were used to inform the actuator's geometries and functional specifications, including the flow channel dimensions, groove placement, and operating ranges. Due to budget constraints, the physical prototype was not fabricated at this stage. Instead, the actuator plate was developed and simulated in ANSYS Fluent to evaluate the local airflow behaviour and shear force generation. Also, system-level parameters such as bandwidth and acceleration were not tested and will remain for future work.

**Table 2. Design system prerequisites [16].**

| System | Parameters | Unit | Value |
|---|---|---|---|
| **Convey and positioning system** | Control bandwidth | $Hz$ | 100 |
| | Acceleration | $m/s^2$ | 1-5 |
| | Bearing stiffness | $N/m \cdot m^2$ | $1 \times 10^7$ |
| **Convey system** | Maximum velocity | $m/s$ | 10 |

### 2.3.1. Actuator plate design

The actuator plate was designed as a modular hexagonal actuator array layout aluminium structure. Its modularity can enable large-scale applications, with each module being an individual building block. An individual module consists of a hexagonal layout of seven actuator cells; each was designed with specific dimensions aimed to generate aerodynamic shear forces for non-contact transport. This represents a more advanced modification of the conventional square or circle actuator design. The actuator plate has dimensions of 35mm (length), 0.8mm (thickness), featuring 7 hexagonal actuator cells. Each actuator cell consists of a 10 mm side hexagonal pocket, 0.2 mm deep, bordered by 2 mm dams. Moreover, six circular ports (2 mm diameter) are positioned around the pocket and connected via 0.8 mm deep and 1.5 mm wide grooves to facilitate airflow distribution.

The final design of the hexagonal actuator plate was exported as a STEP file for CFD simulations. Figure 4 presents the overall dimensions of the actuator plate; the red dots indicate the inlet ports; green dots represent the outlet ports. The actuator plate is designed with a modular hexagonal configuration, allowing it to be seamlessly tiled and scaled up for larger-area applications in industrial conveying systems, shown in Fig. 5.

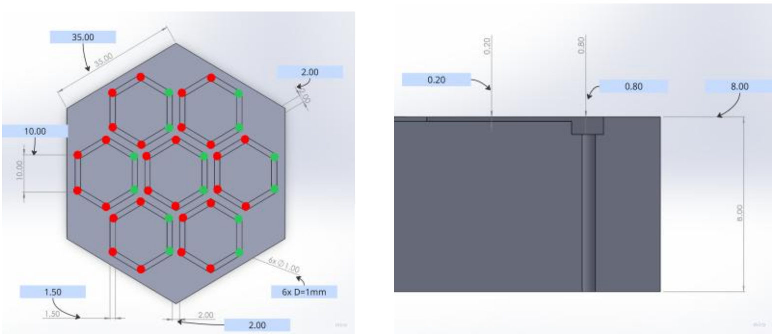


**Fig. 4. Hexagonal actuator plate and section view for pocket.**

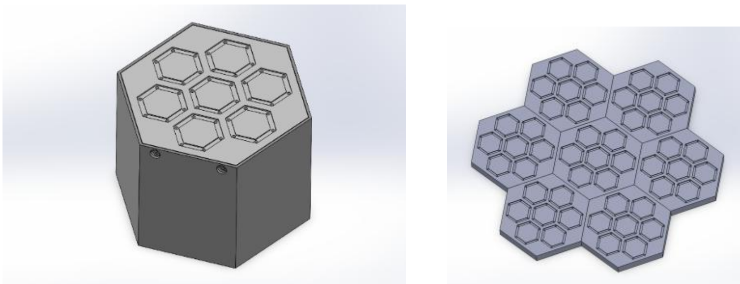

**Fig. 5. HexaFloat individual module (left) and a scale up example of several individual modules combined (right).**

### 2.3.2. Airflow configuration

The airflow control of the HexaFloat system is based on a set of six independently operated fast switch valves, typically 3/2 solenoid valves. Each of the valves is connected to a group of actuator ports sharing the same orientation as Fig. 6 demonstrates. Six colours were used (see Fig. 6) to differentiate the ports controlled by each operating valve. These valves work to selectively switch between pressurized air and vacuum, generating a directional pressure differential that induces shear forces for object movement. By adjusting the supply and suction flow rates, the system can control object acceleration, deceleration, and directional switching. The direction of object movement can be determined by the orientation of the induced airflow, as illustrated in Fig. 6 (b). The small filled red dots indicate ports with positive pressure, while the blue dots indicate ports with negative pressure. Although the control logic was not physically implemented, this configuration provides a theoretical basis for achieving 6-degree-of-freedom (6-DOF) transport and stable levitation in future development.

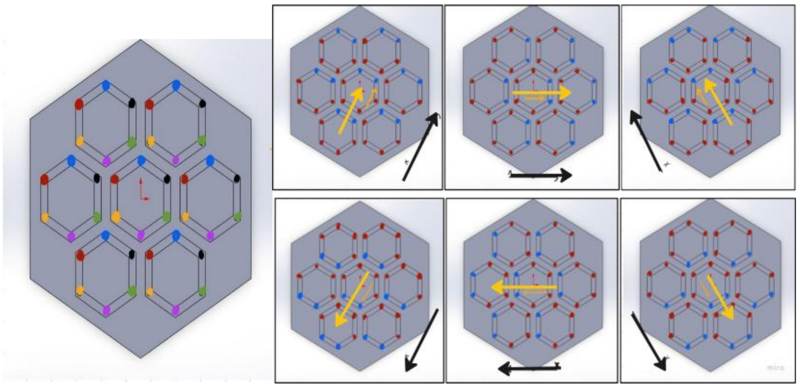

**(a) (b)**

**Fig. 6. Airflow configuration with distinct coloured ports (a) and actuating directions (b).**

## 2.4. Simulation

CFD simulations were conducted using ANSYS Fluent to analyse the airflow dynamics, pressure distribution, and shear forces within the actuator cells. The model was derived from the imported SolidWorks STEP file (Fig. 7). The simulation focused solely on evaluating and optimizing key design parameters such as pocket depth, dam width, groove width, port configurations and etc. The objective was to evaluate the actuator design's capacity to generate stable levitation and controlled shear forces for directional actuation. Moreover, various input configurations were tested, including different air supply setups to evaluate their impact on overall system performance. Further adjustments of the actuator system will be implemented to improve and optimize the efficiency and stability based on the outcome obtained from the simulation. The final design was selected based on achieving a balance between conveying performance and energy efficiency.

In the simulation, the model was not directly applied to the actuator plate. Instead, a fluid domain was created within and above the actuator geometry to visualize airflow entering through the inlet, passing through the pocket, and exiting at the outlet. This domain includes the air volume within the actuator pockets and the thin air film above them, representing the gap between the actuator dam and the base of the transported object, as shown in Fig. 7. The air film height (h) was set to

35 $\mu m$. This is similar to the values reported in literature. It was set for the entire simulation. Subsequently, a structured mesh and inflation layer were utilized, with finer elements concentrated around the pocket, air film, and dam areas, to accurately capture the shear layer and flow behaviour.

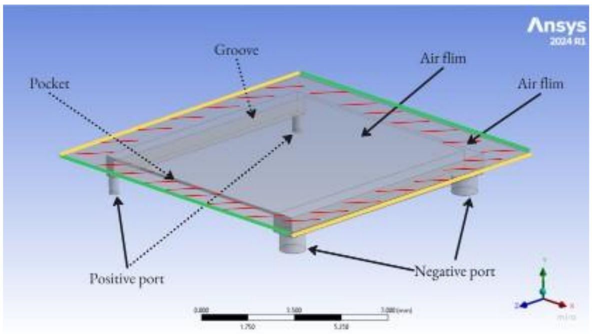


**Fig. 7. Fluid domain created for validation model.**

The CFD simulation applied boundary conditions based on the validated setup. Positive port and negative ports were defined as pressure inlets and outlets to direct airflow through the actuator. All solid surfaces, including port walls, pocket grooves, directional walls (green line), and the dam (shown in red line), were set as no-slip boundaries. The lateral faces of the air film (yellow line) were set as symmetry boundaries. These definitions are crucial for capturing accurate flow behaviour. Next, this simulation approach ensures realistic flow behaviour under low-speed conditions, where the relatively small pressure gradients contrasted to the ambient pressure and low Reynolds number (<1000) justify the use of an incompressible, isothermal, and laminar flow assumption. A uniform pressure distribution across the pocket width was assumed due to the groove design, and a thin-film approximation was applied, as the air film thickness was much smaller than the pocket dimensions.

Various scenarios were conducted to investigate how the key design parameters, such as dam width, groove width, port sizing, and different air supply setups influence the system's performance. These variations were systematically tested to identify the optimal balance between system conveyance performance and operational efficiency. Key performance indicators such as shear (traction) force and volumetric flow rate were evaluated across each configuration and compared to determine the most effective and efficient design.

The first scenario served as the reference for evaluating the performance of the actuator plate. In this configuration, the actuator pocket has a depth of 0.2 mm, and a pressure difference of 500 Pa is applied across the ports. The geometric design included a dam width of 1 mm, a groove width of 1.5 mm, and a port diameter of 1 mm. The air supply layout consisted of 4 inlet ports and 2 outlet ports (4 in/2 out), which represents the standard configuration adopted in the HexaFloat design. It provided the basis for comparison against other modified geometries and airflow conditions, enabling a consistent assessment of how each variation impacts traction force generation and volumetric flow performance. The depth of the actuator pocket remained constant at 0.2 mm. The summaries of the first scenario and other scenarios are listed in Tables 3 and 4, respectively.

**Table 3. Summary of first simulation scenarios.**

| Scenario | Description | $\Delta P$ (Pa) | $P_{in}$ (Pa) | $P_{out}$ (Pa) | Dam Width (mm) | Groove Width (mm) | Port Size (mm) | Port Layout (inlet/outlet) |
|---|---|---|---|---|---|---|---|---|
| 1 | Reference | 500 | 250 | -250 | 1 | 1.5 | 1 | 4 in / 2 out |

**Table 4. Summary of simulation scenarios.**

| Scenario | Description | Setups |
|---|---|---|
| 2 | Different $\Delta P$ | ΔP=250Pa ($P_{in} = 125Pa$; $P_{out} = -125Pa$)<br>ΔP=1000Pa ($P_{in} = 500Pa$; $P_{out} = -500Pa$) |
| 3 | Distinct air supply setup | ΔP=750 ($P_{in} = 250Pa$; $P_{out} = -500Pa$)<br>ΔP=750Pa ($P_{in} = 500Pa$; $P_{out} = -250Pa$) |
| 4 | Different dam width | 2mm, 0.5mm |
| 5 | Wider groove width | Groove width: 2mm |
| 6 | Smaller port sizes and grooves width | Port size: 0.5mm<br>Groove width: 0.7 mm; Port size: 0.5mm |
| 7 | Different port layout | 2 positive ports with 4 negative ports |

## 3. Result and Discussion

### 3.1. Validation of the computational model

The base model was validated against existing literature [16]. CFD simulations and MATLAB analytical modelling were performed, replicating the conditions of a 30-cell actuator array as presented in the reference study. The output parameters, including traction force to the wafer, airflow volume flow rate, and velocity, were computed and compared with theoretical values published in the literature to assess the accuracy of the developed models. Additionally, a new simulation scenario using a pressure difference of ΔP = 250 Pa was introduced to further validate the model beyond the range reported in the original study. The results in Fig. 8 present the theoretical values of traction force and volume flow rate for comparison against the simulation outcomes.

The validation results for a 30-cell actuator array demonstrated agreement between the theoretical and computational models. As Fig. 8 shows, both the traction force and volume flow rate increased consistently with rising pressure difference, confirming the expected behaviour. They exhibited a positive linear trend as the pressure difference increased from 0.25 to 1.00 kPa. A linear regression of the traction force yielded a gradient of 2.58 for simulation and 2.32 for theoretical. The difference of 11.2% indicates agreement between the analytical model and CFD simulation.

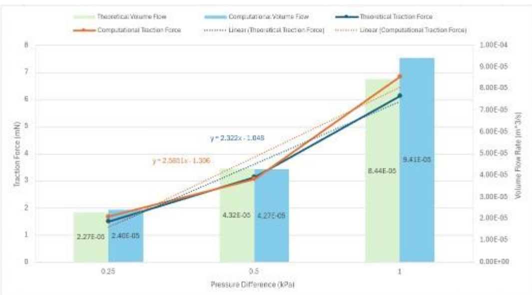


**Fig. 8. Comparison of traction force and volume flow rate between the literature and simulation.**

Figures 9 and 10 show the pressure distribution and flow velocity at ΔP = 0.5 kPa, comparing simulation results with literature. Results revealed a well-defined pressure gradient within the actuator with relatively uniform distribution across each pocket, with the inclusion of grooves improving the pressure uniformity. This indicated the correct setup of boundary conditions. The flow velocity profile closely matched with literature, with a simulated peak velocity of 2.253 m/s versus 2.385 m/s reported, a 5.5% difference.  The results confirm that the simulation and analytical models have replicated actuator behaviour under various pressure conditions.

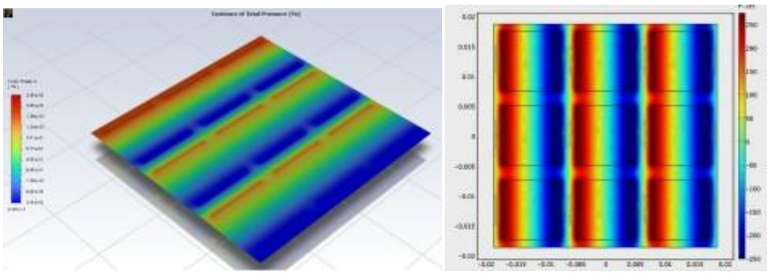

**Fig. 9. Pressure distribution in simulation (left) and literature (right) with ΔP=0.5kPa.**

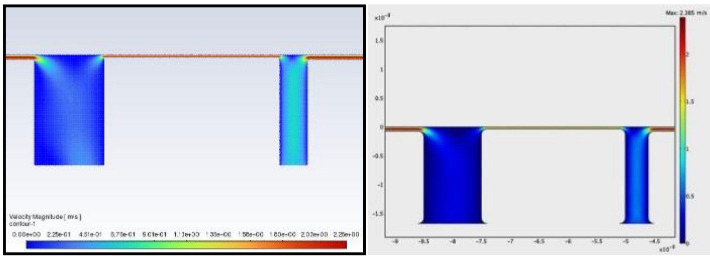

**Fig. 10. Flow velocity in simulation (left) and literature (right) with  ΔP=0.5kPa.**

## 3.2. Simulation result

The HexaFloat actuator plate was simulated with seven different conditions. These conditions involved variations in actuator geometry and air supply configurations. These scenarios were compared to identify the optimal design and supply setup that would enable stable, efficient, and multidirectional object movement.

### 3.2.1. Comparison of square and hexagonal actuator cell geometry

For scenarios 1 and 2, the comparison between a single square actuator cell (literature) and a single HexaFloat (hexagonal) actuator cell under two pressure difference conditions of 500 Pa and 1000 Pa is shown in Fig. 11. The hexagonal geometry consistently outperformed the square cell in traction force by achieving 0.136 mN and 0.174 mN higher than the square cell under the same pressure supply conditions. However, this enhancement comes with a trade-off of exhibiting higher volume flow rates, which are significantly greater than the square. According to the literature, higher flow rate implies increased power consumption of the blower and poses a greater risk of turbulent flow, which could affect the system stability. The reason for higher volume flow rate could be due to larger ports and wider grooves compared to the square cell, under the same ΔP.

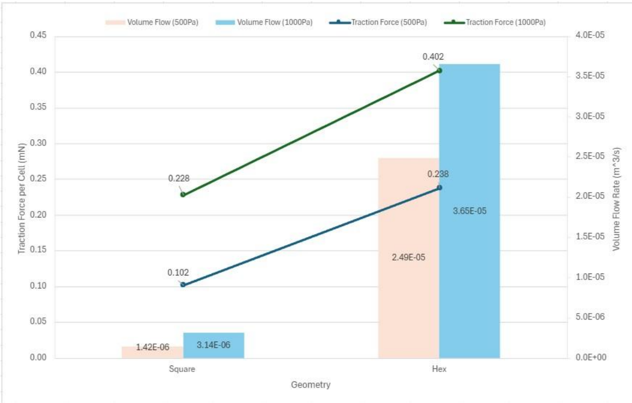


**Fig. 11. Comparison of traction force and volume flow rate between the square and hexagonal actuator cells.**

Moreover, the transition of the hexagon actuator cell can also result in more flow paths. The reason is that the hexagonal geometry is more compact and is tiled with 6 neighbouring directions. This enables airflow to spread and exit more freely, thereby increasing air flow. The additional ports, from four to six ports for the hexagonal layout may also lead to better flow spreading and reducing the pressure drop losses within the pocket. However, the enhanced traction force in the hexagonal cell suggests a higher acceleration capability that is suitable for heavier items. The hexagon actuator cell also allows multidirectional object movement, which is a functional advantage that may justify the additional energy consumption in practical applications.

The pressure distribution of the hexagonal actuator cell with the pressure difference of 500 Pa is shown in Fig. 12. The pressure contour shows a clear gradient from the high-pressure inlet (+250 Pa) to the low-pressure outlet (−150 Pa), confirming effective directional airflow across the hexagonal actuator. While the flow distribution is generally consistent, some asymmetry was observed due to the port layout. Overall, the actuator successfully generated the intended pressure drop to support the shear force, with potential for further uniformity improvements through port or groove adjustments.

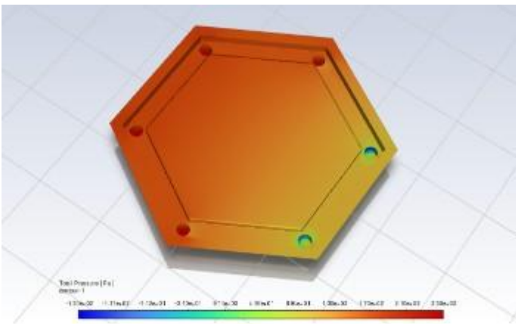

**Fig. 12. Simulated pressure distribution on the HexaFloat actuator cell.**

### 3.2.2. Effect of pressure difference (ΔP) and friction drag coefficient

The comparison of how the air supply pressure difference impacts the system performance was conducted by comparing the results from simulation scenarios 1 and 2. Figure 13 shows, both traction force and volume flow rate rise proportionally with pressure difference, indicating that greater pressure supply difference enhances air momentum and shear force generation. These outcomes aligned with the theoretical understanding that increased driving pressure amplifies airflow velocity, thereby improving shear on the levitated object's surface.

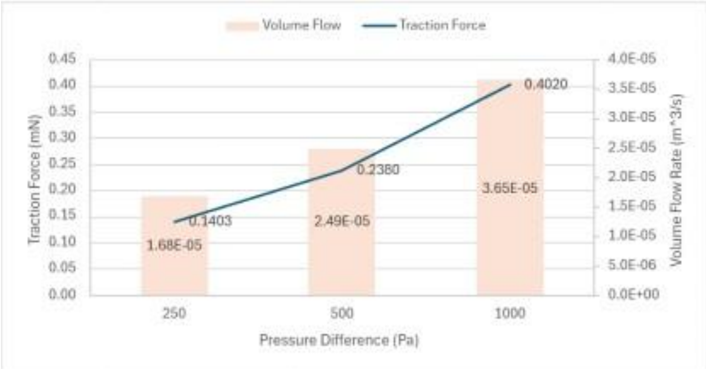


**Fig. 13. Comparison of traction force and volume flow rate under various pressure difference configurations.**

### 3.2.3. Effect of air supply configuration

In scenario 3, both balanced and unbalanced air supply setups were examined. As Fig. 14 shows the variations in inlet and outlet pressure distributions resulted in similar volume flow rates while maintaining a stable traction force. This suggests that the total pressure differences (ΔP) are the primary factor influencing the actuator performance, whereas the specific distribution of air supply between inlet and outlet has a relatively minor effect. These findings highlighted the actuator's robustness to asymmetric air supply conditions, as the traction force remains consistent through different setups.


**Fig. 14. Comparison of traction force and volume flow rate under various pressure supply configurations.**

### 3.2.4. Influence of actuator dam width

For scenario 4, a comparison across various dam widths was conducted to evaluate its effect on the conveyor performance. Based on Fig. 15, the results show that while the traction increases slightly, the volume flow remains constant at different dam geometries. This indicates that dam width affects local shear distribution and potentially increase the effective surface area over which momentum is transferred. However, the influence of dam width is minor in comparison to the pressure difference (ΔP).

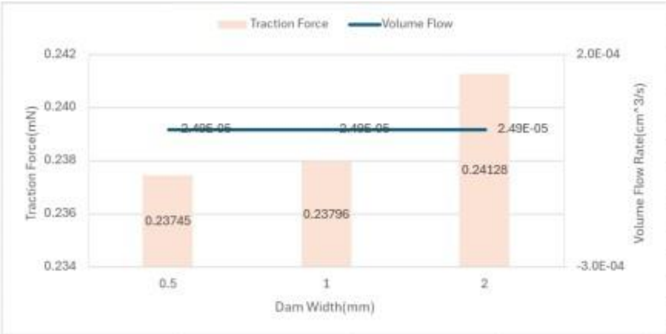


**Fig. 15. Comparison of traction force and volume flow rate with different dam widths.**

### 3.2.5. Influence of actuator groove width

Figure 16 illustrates the comparison of the traction force and volume flow of the actuators with a wider groove. Reducing groove width results in enhanced traction force while maintaining a relatively constant volume flow rate. This shows that narrower grooves help channel airflow more directly toward the central pocket area and the flow direction, thereby minimizing lateral divergence and energy losses. Consequently, greater input airflow contributed to generating effective shear to the object's surface, thus enhancing traction. Moreover, incorporating a narrower groove design appeared to be a beneficial adjustment for improving actuator performance, as the volume flow remained almost unchanged with the reduced width.

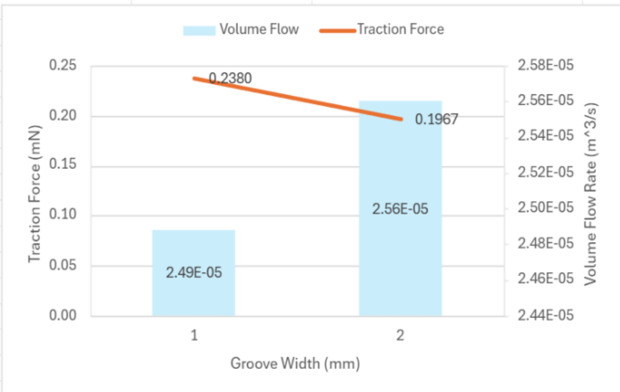


**Fig. 16. Comparison of traction force and volume flow rate with wider groove.**

### 3.2.6. Impact of port diameter

Figure 17 shows the relationship between supply port diameter to actuator performance. It shows that traction force and volume flow rate are greatly boosted by the increase in port diameter. Larger ports reduce inlet resistance, enabling stronger airflow into the pocket and enhancing momentum transfer to the object's surface. Moreover, another benefit of a larger port is that it could create greater vertical stiffness of the conveyor for the objects [16]. An actuator featuring a combination of narrow grooves and 0.5 mm ports was contrasted with an actuator with 0.5 mm ports and wider grooves. The actuator cell with smaller ports and grooves resulted in a slight increase in shear force but reduced volume flow rate as shown in Fig. 18. The result indicates that while flow availability may increase, a mismatch between groove and port sizing can also reduce shear efficiency due to non-optimized flow direction and weaker velocity gradients near the top surface.

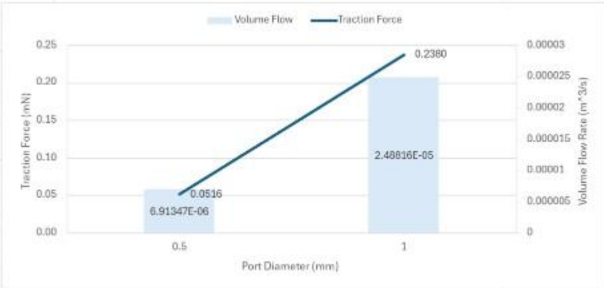


**Fig. 17. Comparison of traction force and volume flow rate with different port sizes.**

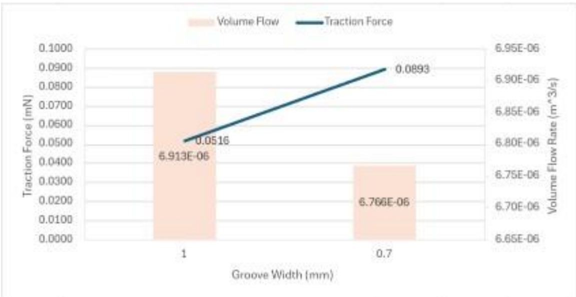


**Fig. 18. Comparison of traction force and volume flow rate with a smaller groove width (0.5mm ports).**

### 3.2.7. Impact of air supply ports layout

In the final simulation scenario, two different air supply port configurations were evaluated. The first setup utilized four positive inlet ports and two negative outlet ports (Fig. 19). In contrast, the second setup reversed this arrangement by employing only two inlet ports while four ports served as outlets under negative pressure (Fig. 19). Figure 20 shows the comparison between different port layouts, indicating that the 2-inlet with 4-outlet configuration attained both higher traction and volume flow rate compared to the 4-inlet with 2-outlet setup. This indicates that increasing the number of outlets relative to inlets reduces back pressure and enhances flow extraction, thereby facilitating more efficient air circulation through the actuator pocket. The enhanced outflow is predicted to minimize stagnation zones and facilitate more efficient directional flow, and result in more effective momentum transfer to the object's surface. Consequently, a balanced or outlet-favoured port layout can improve actuator performance by enhancing both flow distribution and shear force.

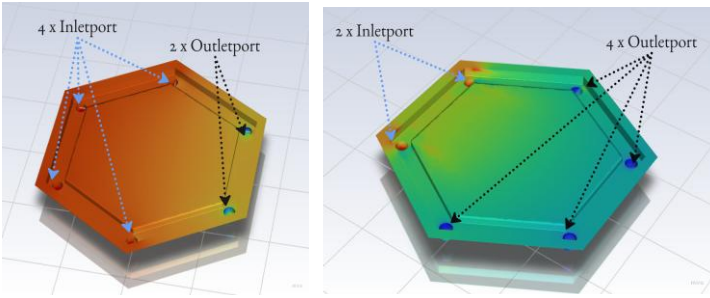


**Fig. 19. Air supply ports configuration for the 1st setup (left) and 2nd setup (right).**

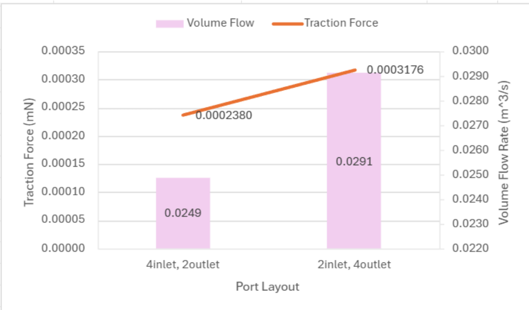


**Fig. 20. Comparison of traction force and volume flow rate with a distinct port setup.**

## 3.3. Summary of simulation and performance evaluation

The simulation results showed that the HexaFloat design met its intended performance objectives. It consistently produced higher traction forces than the conventional square actuators, supported improved acceleration and facilitated multidirectional movement. Additionally, the parametric simulation study showed that pressure difference had the most critical influence on performance, while other factors such as variations in groove width, dam width, port diameter, and port layout can provide additional tuning opportunities to balance shear force with energy efficiency. However, although a few asymmetries in the pressure distribution were observed in the HexaFloat design due to port placement, it could still produce the required pressure drop to generate sufficient shear force. Further improvement in flow uniformity can be achieved through targeted design improvement.

The HexaFloat's significance lies in its modularity, scalability, and suitability for the precision handling of delicate substrates such as wafers and glass sheets in more advanced manufacturing environments. It is hoped that this study has contributed towards developing an aerodynamics traction-based transport system which has the potential for further advancement for it to be used in high-precision, non-contact automation applications.

## 4. Conclusion and Future Work

A novel contactless air conveyor system based on aerodynamic traction principles called HexaFloat was developed and analysed. The simulation model was validated against literature benchmarks and analytical equations. The change from conventional square actuator cells to modular hexagonal cell array shows enhanced traction force performance, enabling multidirectional product movement with increased flexibility. Specifically, the HexaFloat design achieved traction force improvements of approximately 0.136 mN and 0.174 mN higher than the square actuator under pressure differences of 500 Pa and 1000 Pa, respectively. However, this improvement is accompanied by a trade-off in that the hexagonal design exhibited significantly higher volume flow rates, which implied greater airflow demand and higher power consumption. This highlighted the trade-off between improved traction performance and energy efficiency that must be considered in practical deployment.

Based on the parametric simulation results, the pressure difference showed the strongest influence on actuator performance, while geometrical adjustments provided modification options to balance performance and energy consumption. Nevertheless, the hexagonal design's higher volume flow rates, while requiring greater energy consumption, can be justified considering the system's capability of enhanced acceleration and multidirectional movement.

Prototype fabrication and experimental testing are recommended to validate simulation results under real-world conditions, including unexpected leakages, material imperfections, actuator plate surface roughness as well as component tolerances. Moreover, the integration of an active valve-based control system to enable effective 6-DOF manipulation will help to realize the full potential of the HexaFloat. Future research could also focus on controller integration, dynamic objects' response as well as energy optimization strategies to improve the system's scalability and to broaden its applicability for diverse applications.

## References

1. Chandu, L.; Adithya, H.S.; Abhishek, P.; Darshan K.H.S.; and Hemanth K.K.J. (2024). Design and fabrication of contactless air conveyor. *International Journal of Novel Research and Development*, 9(4), f227-f231.
2. Zhong, W.; Gu, X.; Li, X.; and Kagawa, T. (2017). Study on the basic characteristics of a noncontact air conveyor for large glass sheets. *Advances in Mechanical Engineering*, 9(4), 1687814017697190.
3. OCS Overhead Conveyor System Ltd. (2019). Different types of conveyor systems? Retrieved May 20, 2025, from https://ocssystem.co.uk/conveyor-expertise/different-types-of-conveyor-systems/
4. Vuong, P. (2016). *Air-based contactless actuation system for thin substrates: The concept of using a controlled deformable surface*. PhD Thesis, Mechatronic Systems Design, Delft University of Technology.
5. Zhu, L.; El-Baz, D; and Ning, H. (2015). Survey on air levitation conveyors with possible scalability properties. *Proceedings of* 2015 *IEEE* 12*th Intl Conf*

*on Ubiquitous Intelligence and Computing and* 2015 *IEEE* 12*th Intl Conf on Autonomic and Trusted Computing and* 2015 *IEEE* 15*th Intl Conf on Scalable Computing and Communications and Its Associated Workshops (UIC-ATC-ScalCom)*, Beijing, China, 802-807.

6. Andrade, M.A.B.; Pérez, N.; and Adamowski, J.C. (2018). Review of progress in acoustic levitation. *Brazilian Journal of Physics*, 48(2), 190-213.
7. SoftGripping. (2021). A comprehensive guide to grippers. Retrieved May 30, 2025, from https://soft-gripping.com/discover/a-comprehensive-guide-to-grippers/
8. Chen, C.-J.; and DeBra, D.B. (1987). A laminar flow motor for precision machining. *CIRP Annals*, 36(1), 385-390.
9. Paivanas, J.A.; and Hassan, J.K. (1979). Air film system for handling semiconductor wafers. *IBM Journal of Research Development*, 23(4), 361-375.
10. Konishi, S.; and Fujita, H.A. (1994). A conveyance system using air flow based on the concept of distributed micro motion systems. *Journal of Microelectromechanical Systems*, 3(2), 54-58.
11. Fukuta, Y.; Chapuis, Y.-A.; Mita, Y.; and Fujita, H. (2006). Design, fabrication, and control of MEMS-based actuator arrays for air-flow distributed micromanipulation. *Journal of Microelectromechanical Systems*, 15(4), 912-926.
12. Zeggari, R.; Yahiaoui, R.; Malapert, J.; and Manceau, J.-F. (2010). Design and fabrication of a new two-dimensional pneumatic micro-conveyor. *Sensors and Actuators A: Physical*, 164(1-2), 125-130.
13. Delhaes, G.M.J.; van Beek, A.; van Ostayen, R.A.J.; and Schmidt, R.H.M. (2009). The viscous driven aerostatic supported high-speed spindle. *Tribology International*, 42(11-12),1550-1557.
14. Delettre, A.; Laurent, G.J.; and Fort-Piat, N.L. (2010). A new contactless conveyor system for handling clean and delicate products using induced air flows. *Proceedings of* 2010 *IEEE/RSJ International Conference on Intelligent Robots and Systems*, Taipei, Taiwan, 2351-2356.
15. van Rij, J. et al. (2008). Planar flat product transport using viscous traction. *Proceedings of the STLE/ASME* 2008 *International Joint Tribology Conference*, Miami, Florida, USA, 355-357.
16. van Rij, J. et al. (2009). Planar wafer transport and positioning on an air film using a viscous traction principle. *Tribology international*, 42(11-12), 1542-1549.
17. van Ostayen, R.A.J.; van Eijk, J.; and Schmidt, R.H.M. (2012). Contact-less thin substrate transport using viscous traction. *Proceedings of* 2012 *Second Workshop on Design, Control and Software Implementation for Distributed MEMS*, Besancon, France, 14-21.
18. Wesselingh, J. (2011). *Contactless positioning using an active air film*. PhD Thesis, Mechatronic Systems Design, TU Delft.
19. Krijnen, M.E.; van Ostayen, R.A.J.; and HosseinNia, H. (2018). The application of fractional order control for an air-based contactless actuation system. *ISA Transactions*, 82(2018), 172-183.